Computationally Efficient Optimal Switching Sequence Model Predictive Control for Three-Phase Vienna Rectifier Under Balanced and Unbalanced DC Links

Bo Xu, Kaipei Liu, and Xiaohong Ran, *Member, IEEE*

***Abstract*—Unbalanced dc links usually occur when a Vienna rectifier is used as a charger for series-connected battery packs. The redundant vector preselection optimal switching sequence model predictive control (OSS-MPC) scheme does not require weighting factor tuning and is applicable to unbalanced dc links. However, its use is complicated for switching sequence selections and duty cycle calculations. Therefore, this article proposes a computationally efficient OSS-MPC scheme for three-phase Vienna rectifier operating under balanced and unbalanced dc links. The scheme achieves the same performance as that achieved by the redundant vector preselection OSS-MPC scheme, however, its execution is significantly more efficient. In the proposed method, an unbalanced factor is proposed by considering unbalanced dc links, and a look-up table is derived to describe the equivalence relation among the six feasible switching sequences. Then, duty cycles are calculated for only one switching sequence, and the OSS and its duty cycles are reconstructed based on the predefined table. Unlike the redundant vector preselection OSS-MPC scheme, the enumeration process is eliminated in the proposed method, thus, the computational burden is significantly reduced. Experimental results are provided to validate the effectiveness of the proposed method. This article is accompanied by a PDF demonstrating the look-up tables.**

***Index Terms*—Duty cycle reconstruction, optimal switching sequence model predictive control (OSS-MPC), three-phase Vienna rectifier, unbalanced dc links, voltage vector reselection.**

I. Introduction

THREE-PHASE Vienna rectifiers are widely used in telecommunication power systems [1], power factor correction systems [2], and wind turbine systems [3]. Compared with a conventional two-level pulsewidth modulation (PWM) rectifier, the three-phase three-level Vienna rectifier has attracted significant attention due to its advantages of low cost, low total harmonic distortion (THD) of input currents, high power density, and high efficiency [1].

As there are two dc-link capacitors in a Vienna rectifier, it is necessary to control both the input ac current and neutral-point voltage. To achieve these two control goals, several representative control methods are introduced as follows. The pioneering work in [1] proposes a hysteresis control method for ac current, and the neutral-point voltage is balanced by injecting zero-sequence current. Then, control methods using carrier-based PWM (CBPWM) [4]–[6], and space-vector PWM (SVPWM) [7] [8] are proposed. Although the above-mentioned methods achieve good performance with respect to both the ac current and neutral-point voltage, the unbalanced dc links are not considered. As mentioned in [9]–[14], a Vienna rectifier may need to operate with unbalanced dc links in some operation scenarios, such as in the transient state or sudden changes in dual dc loads [12]. Moreover, when a Vienna rectifier is used as a one-stage battery charger to improve efficiency and reduce implementation costs, two propulsion battery packs are required to be connected in series to achieve the voltage rating of the Vienna rectifier. The various types and discrepant states of charge result in diverse properties of batteries in terms of C-rates and terminal charging voltages. Thus, unbalanced dc links are inevitable for a Vienna rectifier [13]. When a Vienna rectifier operates under unbalanced dc links, the above-mentioned PWM-based methods are difficult to use, since the magnitude and phase of some voltage vectors vary due to the unbalanced dc links [14]. Some improved modulation schemes are proposed in [9], [12], and [13]. However, these methods usually require complicated calculations since the space-vector diagrams become asymmetric due to the unbalanced dc links. In addition, these PWM methods are usually combined with proportional-integral (PI) control. According to [15], a Vienna rectifier is a highly constrained system, i.e., the control input for a Vienna rectifier is determined by both switching states of power switches and the ac current polarity. As a commonly used PI controller cannot operate with such constraints directly, it is difficult to obtain high performance.

By directly considering the inherent constraints of converters, the model predictive control (MPC) method has emerged as a

Manuscript received November 15, 2020; revised February 6, 2021 and April 15, 2021; accepted May 13, 2021. Date of publication May 20, 2021; date of current version July 30, 2021. This work was supported in part by the National Natural Science Foundation of China under Grant 51607125, and in part by the State Grid Hubei Electric Power Company Technology Program (52153817000N). Recommended for publication by Associate Editor P. Mattavelli. *(Corresponding author: Kaipei Liu.)*

The authors are with the School of Electrical Engineering and Automation, Wuhan University, Wuhan 430072, China (e-mail: 2016202070016@whu.edu.cn; kpliu@whu.edu.cn; xhran@whu.edu.cn).

This article has supplementary material provided by the authors and color versions of one or more figures available at https://doi.org/10.1109/TPEL.2021.3081771.

Digital Object Identifier 10.1109/TPEL.2021.3081771

powerful alternative to conventional control methods due to its advanced properties such as straightforward implementation, flexible design, and fast control dynamics [14]. The existing MPC methods for a Vienna rectifier can be divided into two categories, including the optimal switching vector MPC (OSV-MPC) [15]–[19] and optimal switching sequence MPC (OSS-MPC) [3], [20], [21] methods. For the OSV-MPC method, only one voltage vector is used in a control period [15]–[19]. For example, in [15], the future ac current and neutral-point voltage values are predicted based on the system model of the Vienna rectifier. By defining the cost function as the sum of the ac current and neutral-point voltage terms, with a weighting factor, eight voltage vectors are enumerated in every control period, and the optimal vector with the minimum cost function is adopted as the control input. Although good dynamic performance and a wide operating range are achieved, variable switching frequency and large current ripple are the main drawbacks of the OSV-MPC method. To achieve fixed switching frequency and improve the steady-state performance, the OSS-MPC method is proposed, in which multiple voltage vectors are used in a control period. In [3], an improved discrete SVPWM MPC (DSVM-MPC) method is proposed, and an optimized voltage vector selection principle is adopted to reduce the number of voltage vector candidates. However, this magnitude-based optimized voltage vector selection principle is no longer valid when the Vienna rectifier operates under unbalanced dc links, because the magnitude of the synthesized virtual vectors is dependent not only on the dc-link voltage but also on the difference between the two capacitor voltages. In [20], a cost function-based modulation MPC (CFM-MPC) method is proposed. This method is applicable to unbalanced dc links. However, the neutral-point voltage is regulated by adding a neutral-point voltage term with a weighting factor in the cost function. As mentioned in [22], an appropriate weighting factor is difficult to design. In [21], the redundant vector preselection OSS-MPC (RVP-OSS-MPC) method is proposed for a Vienna rectifier. The redundant vector that causes the neutral-point voltage to approach zero is preselected. Then, the six feasible switching sequence candidates are enumerated, and the OSS with the minimum cost function is adopted as the control input. Compared with the DSVM-MPC [3] and CFM-MPC [20] methods, the RVP-OSS-MPC method in [21] eliminates the weighting factor tuning. Moreover, it is also applicable for unbalanced dc links. However, the computational burden of RVP-OSS-MPC is large due to the enumeration process of six switching sequences.

In fact, reducing the high computational burden caused by enumeration-based predictions has become an important issue to consider while using the OSS-MPC method [23]. It can lead to a faster controller and shorter sampling time, which improves the current quality of the converter [24]. Moreover, other functions can be included, such as the speed measurement or observer algorithms to improve the system robustness [25], [26]. The computational burden reduction methods can be divided into three categories. The first category optimizes the derivation of the duty cycles [20]. However, the duty cycles are obtained based on cost function value minimization rather than tracking error minimization. Thus, the reference tracking performance cannot be guaranteed [14], [27]. The second category uses a dead-beat type OSS-MPC method [23], [27]–[30]. The reference voltage vector is calculated and then used to simplify the switching sequence selections and duty cycle calculations. However, when applying this method to the unbalanced dc links, nonoptimal switching sequence might be selected frequently due to the asymmetric space-vector diagram, and the ac current becomes distorted [14]. The third category is based on the equivalence relation between different switching sequences [31]–[33]. In [31], the duty cycles are calculated for only one switching sequence, and the OSS and its duty cycles are reconstructed according to a predefined table. No complex trigonometric function is required, and satisfactory performance is achieved. However, only a three-phase two-level converter is considered in [31]–[33]. When a Vienna rectifier operates under unbalanced dc links, the equivalence relation between different switching sequences in [31]–[33] (refer to in [31, eq. (38)]) is not applicable. To solve this problem, an unbalanced factor is proposed in this article. Thus, low THD of the ac current and low computational burden are achieved simultaneously.

In this article, a computationally efficient OSS-MPC scheme for a three-phase Vienna rectifier under balanced/unbalanced dc links is investigated. The main contributions of this article are summarized as follows.

1) A computationally efficient OSS-MPC scheme is proposed. The weighting factor for neutral-point voltage control is eliminated, and this scheme is applicable to balanced and unbalanced dc links.
2) Different from [31]–[33], this article further considers the unbalanced dc links in the Vienna rectifier and proposes an unbalanced factor. Based on the unbalanced factor, a look-up table is established to describe the equivalence relation among the six feasible switching sequences of the Vienna rectifier. Then, the duty cycles are calculated for only one switching sequence, and the OSS and its duty cycles are correctly reconstructed based on the predefined table. Unlike the RVP-OSS-MPC method in [21], the enumeration process is eliminated in the proposed method. Therefore, the proposed method achieves the same performance as that achieved by the RVP-OSS-MPC method [21], whereas the computational burden is reduced from 24.6 μs [21] to 4.7 μs (for the proposed method). Compared with other computational burden reduction methods (see [20], [27], [29], and [30]), the proposed method achieves better current quality under unbalanced dc links. Specifically, when the neutral-point voltage is 50 V, the current THD is reduced from 5.31% (for the low complexity MPC [27]) to 2.85% (for the proposed method).
3) As a Vienna rectifier comprises 6 sectors, and 2 redundant vectors in each sector, a comprehensive analysis of the 12 situations with different sectors and preselected redundant vectors is conducted. Four look-up tables are obtained to describe the equivalence relation among the feasible switching sequences of these twelve situations, which ensures that the increased memory usage of the proposed method is limited.

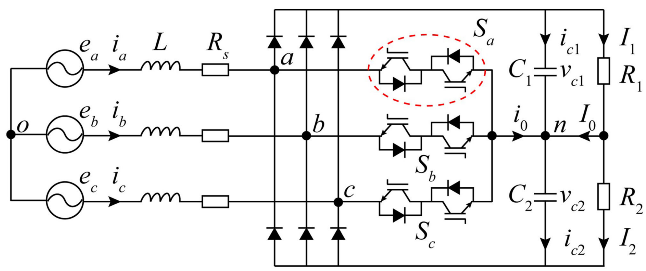

Fig. 1. Topology of three-phase Vienna rectifier.

The remainder of this article is organized as follows: Section II presents the system model of a Vienna rectifier. In Section III, the proposed method is described in detail. In Section IV, the experimental results are presented and discussed. Finally, the conclusion is drawn in Section V.

II. Model of Three-Phase Vienna Rectifier

The topology of a three-phase Vienna rectifier is shown in Fig. 1, which consists of a three-phase diode bridge, three bidirectional switches, three boost inductors, and two dc capacitors.

For the ac side of a Vienna rectifier, the grid current dynamics in the three-phase stationary reference frame (*a-b-c*) are expressed as

$$L\frac{di_x}{dt} = e_x - R_s i_x - v_{xn} - v_{no}, x = a, b, c \quad (1)$$

where e_x, i_x, and v_{xn} are the *x*-phase grid voltage, *x*-phase grid current, and the output *x*-phase voltage (referred to neutral point *n*) generated by the Vienna rectifier, respectively. L is the input inductance, R_s is the equivalent input resistance, and v_{no} is the zero-sequence voltage.

Due to the operational characteristics of the Vienna rectifier, v_{xn} is determined not only by the switching states of three bidirectional switches, but also by the direction of input ac current. Thus, v_{xn} can be expressed as

$$v_{xn} = (1 - S_x)\left(\frac{\text{sign}(i_x) + 1}{2}v_{c1} + \frac{\text{sign}(i_x) - 1}{2}v_{c2}\right) \quad (2)$$

where sign(.) is the sign function, and v_{c1} and v_{c2} are the voltages across the dc-link capacitors C_1 and C_2, respectively. S_x ($x =$ *a*,*b*,*c*) is the switching states of the three bidirectional switches. $S_x = 0$ indicates the switch S_x is OFF, and $S_x = 1$ indicates the switch S_x is ON.

From (1), the state-space equation of a Vienna rectifier in the two-phase stationary reference frame (α–β) can be obtained as

$$\begin{aligned}\frac{di_\alpha}{dt} &= \frac{1}{L}(e_\alpha - R_s i_\alpha - v_\alpha)\\ \frac{di_\beta}{dt} &= \frac{1}{L}(e_\beta - R_s i_\beta - v_\beta)\end{aligned} \quad (3)$$

where i_α, i_β, e_α, e_β, v_α, and v_β are the grid current, grid voltage, and output voltage generated by a Vienna rectifier in the α–β coordinate, respectively.

For the dc side of the Vienna rectifier, it is assumed that $C_1 = C_2 = C$, and neutral-point voltage v_{np} is defined as the difference

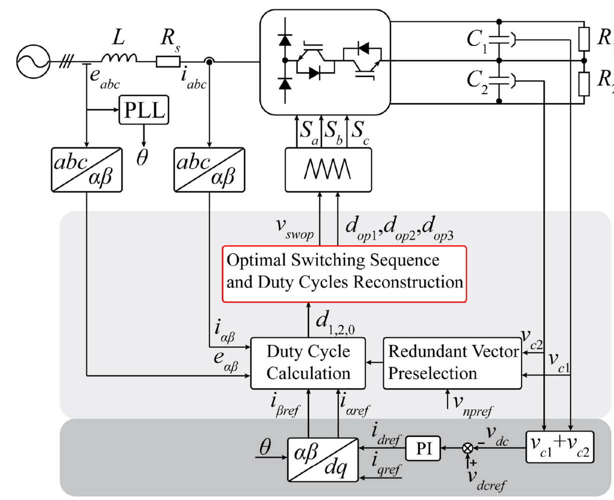

Fig. 2. Block diagram of the proposed control scheme.

between v_{c1} and v_{c2}

$$v_{\text{np}} = v_{c1} - v_{c2}. \quad (4)$$

The dynamics of v_{np} can be expressed as

$$C\frac{dv_{\text{np}}}{dt} = i_{c1} - i_{c2} = -i_0 - I_0 \quad (5)$$

where i_{c1} and i_{c2} are the current passing through C_1 and C_2, respectively, and i_0 is the neutral-point current. Due to the unbalanced dc links, the current I_1 supplied by C_1 to load R_1 may be different from the current I_2 supplied by C_2 to load R_2, and I_o is equal to $I_1 - I_2$.

III. Proposed Computationally Efficient OSS-MPC

Fig. 2 shows the proposed computationally efficient OSS-MPC block diagram for a Vienna rectifier. The dc-link voltage is regulated by the outer PI loop. To generate balanced/unbalanced dc links, neutral-point voltage reference v_{npref} is introduced. For example, if $v_{\text{npref}} = 0$, balanced dc links are obtained. If v_{npref} is greater or smaller than 0, unbalanced dc links are obtained, and v_{c1} is greater or smaller than v_{c2}, respectively. In the inner loop, the neutral-point voltage control and ac current control are divided into two steps. In the first step, the redundant vector that regulates v_{np} to v_{npref} is preselected as the method depicted in [21]. In the second step, the proposed method calculates the duty cycles for only one switching sequence, and the OSS and its duty cycles are reconstructed based on a predefined table. Detailed descriptions of each part are given in the following text.

A. Neutral-Point Voltage Control

Depending on the polarity of three-phase ac current, the operation region of the Vienna rectifier is divided into six sectors [3]. In the following analysis, sector I is taken as an example to demonstrate the proposed method, and the other sectors can be analyzed similarly.

When $i_a>0$, $i_b<0$, and $i_c<0$, it indicates that the Vienna rectifier operates at sector I. The space vector diagrams of a Vienna rectifier in sector I with balanced/unbalanced dc links

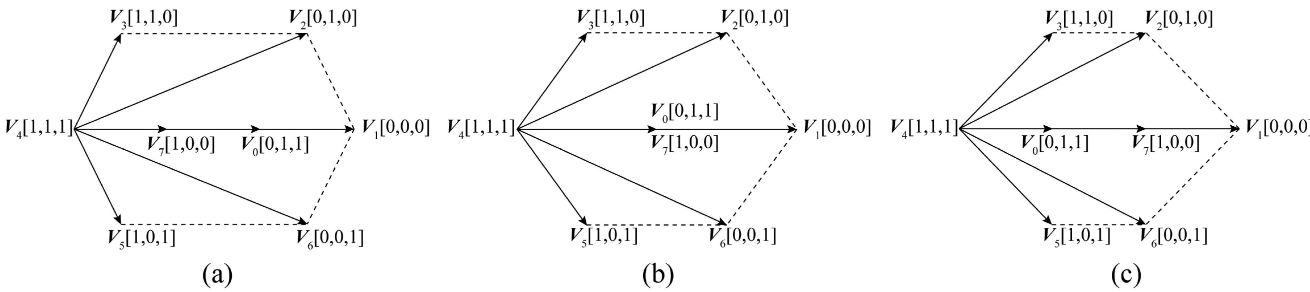

Fig. 3. Space vector diagrams of three-phase Vienna rectifier in sector I under balanced and unbalanced dc links. (a) $v_{c1} > v_{c2}$. (b) $v_{c1} = v_{c2}$. (c) $v_{c1} < v_{c2}$.

are shown in Fig. 3. As seen in Fig. 3, there are eight voltage vectors $\boldsymbol{V}_0, \boldsymbol{V}_1, \ldots, \boldsymbol{V}_7$. $\boldsymbol{V}_0$ and $\boldsymbol{V}_7$ are called redundant vectors as they have the opposite effect on the neutral-point voltage. Besides, the switching states of each voltage vector are also listed out in Fig. 3. For example, $\boldsymbol{V}_0$ [0, 1, 1] indicates that the switching states of S_a, S_b, and S_c are 0, 1, and 1, respectively.

Instead of using a single voltage vector in OSV-MPC, multiple voltage vectors are used in OSS-MPC. For switching sequence selection, three nearest voltage vectors are typically employed in CBPWM and SVPWM [34]. Due to the presence of redundant vectors, there are two types of switching sequence, which are a five-segment switching sequence and a seven-segment switching sequence [35]. For a five-segment switching sequence, only one redundant vector is used in a control period, and the switching state of one converter phase is maintained without change per control period. Thus, the power loss is reduced, whereas the neutral-point voltage ripple is relatively large. For a seven-segment switching sequence, two redundant vectors are used in a control period. Thus, the neutral-point voltage ripple is reduced, whereas the power loss is increased due to the increased switching frequency. Moreover, if the Vienna rectifier operates under unbalanced dc links, the effects of $\boldsymbol{V}_0$ and $\boldsymbol{V}_7$ on ac current are different, as shown in Fig. 3. As a result, if the neutral-point voltage control method in [14] and [35] is adopted, the synthesized voltage vector may be inaccurate, and the ac current performance is deteriorated. Hence, a five-segment switching sequence is adopted in this article, and the neutral-point voltage is regulated by preselecting one redundant vector per control period as in [21].

According to (5), the neutral-point voltage error dynamics can be expressed as

$$\begin{aligned} C\tfrac{de_{v\mathrm{np}}}{dt} &= -i_0 - I_0 \\ e_{v\mathrm{np}} &= v_{\mathrm{np}} - v_{\mathrm{npref}} \end{aligned} \tag{6}$$

where $e_{v\mathrm{np}}$ is the neutral-point voltage error.

Since I_0 is dependent on v_{c1}, v_{c2}, R_1, R_2, the adjustable control variable for $e_{v\mathrm{np}}$ is i_0. To select the proper redundant vector, it is required that $e_{v\mathrm{np}} i_0 > 0$. In sector I, i_a>0, i_b<0, i_c<0, and the switching states of $\boldsymbol{V}_0$ denote $S_a = 0$, $S_b = 1$, and $S_c = 1$, and i_o is smaller than 0 in this case. Therefore, if $e_{v\mathrm{np}}$<0, the preselected redundant vector should be $\boldsymbol{V}_0$. Similarly, if $e_{v\mathrm{np}}$>0, the preselected redundant vector should be $\boldsymbol{V}_7$.

The six feasible switching sequences ($v_{\mathrm{sw1}}, v_{\mathrm{sw2}}, \ldots, v_{\mathrm{sw6}}$) in sector I with $\boldsymbol{V}_0$ or $\boldsymbol{V}_7$ preselected are listed out in Table I, and the next step is to determine the OSS and its duty cycles for ac current control. To simplify the following analysis, $\boldsymbol{V}_0$ is assumed to be the preselected redundant vector in sector I, and the case in which $\boldsymbol{V}_7$ is preselected can be analyzed similarly.

TABLE I
SIX FEASIBLE SWITCHING SEQUENCES IN SECTOR I

V_0 as pre-selected redundant vector	V_7 as pre-selected redundant vector
v_{sw1}={V_1, V_2, V_0}	v_{sw1}={V_1, V_2, V_7}
v_{sw2}={V_2, V_3, V_0}	v_{sw2}={V_2, V_3, V_7}
v_{sw3}={V_3, V_4, V_0}	v_{sw3}={V_3, V_4, V_7}
v_{sw4}={V_4, V_5, V_0}	v_{sw4}={V_4, V_5, V_7}
v_{sw5}={V_5, V_6, V_0}	v_{sw5}={V_5, V_6, V_7}
v_{sw6}={V_6, V_1, V_0}	v_{sw6}={V_6, V_1, V_7}

B. AC Current Control

1) Limitation of RVP-OSS-MPC: The RVP-OSS-MPC method for a Vienna rectifier is proposed in [21]. In RVP-OSS-MPC, six feasible switching sequences are obtained by preselecting the redundant vector. The optimal duty cycles for each switching sequence are solved by minimizing input current tracking error. After enumerating the six feasible switching sequences, the OSS with the minimum cost function is used to control the Vienna rectifier.

According to (3), the following equations are obtained:

$$\begin{aligned} s_{\alpha j} &= \frac{1}{L}(e_\alpha - R_s i_\alpha - v_{\alpha j}) \\ s_{\beta j} &= \frac{1}{L}(e_\beta - R_s i_\beta - v_{\beta j}) \end{aligned} \tag{7}$$

where $s_{\alpha j}$ and $s_{\beta j}$ (j = 0,1,…,7) are the α–β axis current variation rates for $\boldsymbol{V}_j$. $v_{\alpha j}$ and $v_{\beta j}$ are the α–β axis voltage components for $\boldsymbol{V}_j$.

Taking v_{sw1} as an example, and assuming that the duty cycles of $\boldsymbol{V}_1$, $\boldsymbol{V}_2$, and $\boldsymbol{V}_0$ are d_1, d_2, and d_0, the predicted currents are expressed as

$$\begin{aligned} i_\alpha(k+1) &= i_\alpha(k) + T_s \sum_{j=0}^{2} s_{\alpha j} d_j \\ i_\beta(k+1) &= i_\beta(k) + T_s \sum_{j=0}^{2} s_{\beta j} d_j \end{aligned} \tag{8}$$

where $i_\alpha(k+1)$ and $i_\beta(k+1)$ are the predicted α–β axis currents at the (k+1)th control period, $i_\alpha(k)$ and $i_\beta(k)$ are the sampled

α–β axis currents at the kth control period, and T_s is the control period.

The cost function g in this article is defined as

$$g = (i_{\alpha\mathrm{ref}}(k+1) - i_\alpha(k+1))^2 + (i_{\beta\mathrm{ref}}(k+1) - i_\beta(k+1))^2 \quad (9)$$

where $i_{\alpha\mathrm{ref}}(k+1)$ and $i_{\beta\mathrm{ref}}(k+1)$ are the α–β axis current references at the $(k+1)$th control period.

To minimize the cost function g within one control period, d_1, d_2, and d_0 in (8) are determined by the least-square optimization method, that is

$$\begin{cases} \frac{\partial g}{\partial d_1} = 0 \\ \frac{\partial g}{\partial d_2} = 0 \end{cases}. \quad (10)$$

This yields the following optimal duty cycles:

$$\begin{aligned} d_1 &= \frac{(s_{\beta 2}-s_{\beta 0})\Delta i_\alpha + (s_{\alpha 0}-s_{\alpha 2})\Delta i_\beta + (s_{\alpha 2}s_{\beta 0}-s_{\alpha 0}s_{\beta 2})T_s}{T_s((s_{\beta 2}-s_{\beta 0})s_{\alpha 1}+(s_{\beta 0}-s_{\beta 1})s_{\alpha 2}+(s_{\beta 1}-s_{\beta 2})s_{\alpha 0})} \\ d_2 &= \frac{(s_{\beta 0}-s_{\beta 1})\Delta i_\alpha + (s_{\alpha 1}-s_{\alpha 0})\Delta i_\beta + (s_{\alpha 0}s_{\beta 1}-s_{\alpha 1}s_{\beta 0})T_s}{T_s((s_{\beta 2}-s_{\beta 0})s_{\alpha 1}+(s_{\beta 0}-s_{\beta 1})s_{\alpha 2}+(s_{\beta 1}-s_{\beta 2})s_{\alpha 0})} \\ d_0 &= 1 - d_1 - d_2 \\ \Delta i_\alpha &= i_{\alpha ref}(k+1) - i_\alpha(k) \\ \Delta i_\beta &= i_{\beta ref}(k+1) - i_\beta(k). \end{aligned} \quad (11)$$

After solving d_1, d_2, and d_0, the cost function g for switching sequence v_{sw1} is obtained using (8) and (9). Since there are six feasible switching sequences (v_{sw1}, v_{sw2}, …, v_{sw6}), (8), (9), and (11) are evaluated six times to determine the OSS with the minimum cost function and its duty cycles, which inevitably results in large computational burden.

2) Proposed Computationally Efficient OSS-MPC: To reduce the computational burden of RVP-OSS-MPC, this article proposes a computationally efficient OSS-MPC scheme, which achieves the same performance as that achieved by RVP-OSS-MPC, but executes in a much more efficient way. By considering the balanced/unbalanced dc links, an unbalanced factor is proposed, and a look-up table is obtained to describe the equivalence relation among the six feasible switching sequences. Therefore, the proposed method calculates the duty cycles for only one switching sequence, and the OSS and its duty cycles are reconstructed based on the predefined table. Again, it is assumed that the Vienna rectifier operates in sector I, and $\boldsymbol{V}_0$ is the preselected redundant vector.

An unbalanced factor φ ($\varphi>0$) is defined as

$$\varphi = \frac{v_{c2}}{v_{c1}} \quad (12)$$

where $\varphi = 1$ represents that the Vienna rectifier operates under balanced dc links. If φ is greater or smaller than 1, the Vienna rectifier operates under unbalanced dc links, and v_{c2} is greater or smaller than v_{c1}, respectively. By defining the unbalanced factor φ, the equivalence relation between different switching sequences is described using φ and v_{c1}, which facilitates the following analysis.

Taking v_{sw1} and v_{sw5} as an example, and the following equations are obtained:

$$\begin{aligned} v_{\alpha 0} &= \frac{2}{3}v_{c1}, v_{\beta 0} = 0 \\ v_{\alpha 1} &= \frac{1}{3}(2+2\varphi)v_{c1}, v_{\beta 1} = 0 \\ v_{\alpha 2} &= \frac{1}{3}(2+\varphi)v_{c1}, v_{\beta 2} = \frac{\sqrt{3}}{3}\varphi v_{c1} \\ v_{\alpha 5} &= \frac{1}{3}\varphi v_{c1}, v_{\beta 5} = -\frac{\sqrt{3}}{3}\varphi v_{c1} \\ v_{\alpha 6} &= \frac{1}{3}(2+\varphi)v_{c1}, v_{\beta 6} = -\frac{\sqrt{3}}{3}\varphi v_{c1} \end{aligned} \quad (13)$$

where $v_{\alpha j}$ and $v_{\beta j}$ (j = 0,1,2,5,6) represent the α–β axis voltage components for voltage vector $\boldsymbol{V}_j$ (j = 0,1,2,5,6).

According to (7), the α–β axis current variation rates $s_{\alpha j}$ and $s_{\beta j}$ of $\boldsymbol{V}_j$ (j = 0,1,2,5,6) are derived as

$$\begin{aligned} s_{\alpha 0} &= -\frac{1}{3L}2v_{c1} + s_1, s_{\beta 0} = s_2 \\ s_{\alpha 1} &= -\frac{1}{3L}(2+2\varphi)v_{c1} + s_1, s_{\beta 1} = s_2 \\ s_{\alpha 2} &= -\frac{1}{3L}(2+\varphi)v_{c1} + s_1, s_{\beta 2} = -\frac{\sqrt{3}}{3L}\varphi v_{c1} + s_2 \\ s_{\alpha 5} &= -\frac{1}{3L}\varphi v_{c1} + s_1, s_{\beta 5} = \frac{\sqrt{3}}{3L}\varphi v_{c1} + s_2 \\ s_{\alpha 6} &= -\frac{1}{3L}(2+\varphi)v_{c1} + s_1, s_{\beta 6} = \frac{\sqrt{3}}{3L}\varphi v_{c1} + s_2 \\ s_1 &= \frac{1}{L}(e_\alpha - R_s i_\alpha), s_2 = \frac{1}{L}(e_\beta - R_s i_\beta). \end{aligned} \quad (14)$$

To implement the proposed method, it is necessary to show that $s_{\alpha 5}$, $s_{\beta 5}$, $s_{\alpha 6}$, $s_{\beta 6}$, $s_{\alpha 0}$, and $s_{\beta 0}$ can be reconstructed using $s_{\alpha 1}, s_{\beta 1}, s_{\alpha 2}, s_{\beta 2}, s_{\alpha 0}$, and $s_{\beta 0}$. As the sum of the duty cycles for the selected switching sequence should be 1, it is assumed that the duty cycles for v_{sw1}, $\{\boldsymbol{V}_1, \boldsymbol{V}_2, \boldsymbol{V}_0\}$ are d_1, d_2, and $1-d_1-d_2$, and duty cycles for v_{sw5}, $\{\boldsymbol{V}_5, \boldsymbol{V}_6, \boldsymbol{V}_0\}$ are d_5, d_6, and $1-d_5-d_6$. The α–β axis current variations in a control period caused by v_{sw1}, $\{\boldsymbol{V}_1, \boldsymbol{V}_2, \boldsymbol{V}_0\}$, and v_{sw5}, $\{\boldsymbol{V}_5, \boldsymbol{V}_6, \boldsymbol{V}_0\}$ can be expressed as

$$\begin{aligned} \begin{bmatrix} s_{\alpha\mathrm{vr1}} \\ s_{\beta\mathrm{vr1}} \end{bmatrix} &= T_s \begin{bmatrix} s_1 \\ s_2 \end{bmatrix} - \frac{v_{c1}T_s}{3L} \begin{bmatrix} 2\varphi & \varphi \\ 0 & \sqrt{3}\varphi \end{bmatrix} \begin{bmatrix} d_1 \\ d_2 \end{bmatrix} \\ &\quad - \frac{v_{c1}T_s}{3L} \begin{bmatrix} 2 \\ 0 \end{bmatrix} \\ \begin{bmatrix} s_{\alpha\mathrm{vr5}} \\ s_{\beta\mathrm{vr5}} \end{bmatrix} &= T_s \begin{bmatrix} s_1 \\ s_2 \end{bmatrix} - \frac{v_{c1}T_s}{3L} \begin{bmatrix} \varphi - 2 & \varphi \\ -\sqrt{3}\varphi & -\sqrt{3}\varphi \end{bmatrix} \begin{bmatrix} d_5 \\ d_6 \end{bmatrix} \\ &\quad - \frac{v_{c1}T_s}{3L} \begin{bmatrix} 2 \\ 0 \end{bmatrix} \end{aligned} \quad (15)$$

where $s_{\alpha\mathrm{vr1}}$, $s_{\beta\mathrm{vr1}}$, $s_{\alpha\mathrm{vr5}}$, and $s_{\beta\mathrm{vr5}}$ are α–β axis current variations of the switching sequences v_{sw1} and v_{sw5} in a control period, respectively.

By making $s_{\alpha \mathrm{vr}1}$ and $s_{\beta \mathrm{vr}1}$ equal to $s_{\alpha \mathrm{vr}5}$ and $s_{\beta \mathrm{vr}5}$, respectively, the following equation is obtained:

$$\begin{bmatrix} 2\varphi & \varphi \\ 0 & \sqrt{3}\varphi \end{bmatrix} \begin{bmatrix} d_1 \\ d_2 \end{bmatrix} = \begin{bmatrix} \varphi - 2 & \varphi \\ -\sqrt{3}\varphi & -\sqrt{3}\varphi \end{bmatrix} \begin{bmatrix} d_5 \\ d_6 \end{bmatrix}. \tag{16}$$

From (16), it is observed that the right-side coefficient matrix is always invertible unless $\varphi = 0$. It is not practical, because v_{c2} will be 0 if φ is 0. By solving (16), the following equation is obtained:

$$\begin{aligned} d_5 &= -\varphi d_1 - \varphi d_2 \\ d_6 &= \varphi d_1 + (\varphi - 1) d_2. \end{aligned} \tag{17}$$

It is clearly visible in (17) that the effects of $\boldsymbol{V}_5 d_5 T_s + \boldsymbol{V}_6 d_6 T_s + \boldsymbol{V}_0 (1 - d_5 - d_6) T_s$ are equal to the synthesis of $\boldsymbol{V}_1 d_1 T_s + \boldsymbol{V}_2 d_2 T_s + \boldsymbol{V}_0 (1 - d_1 - d_2) T_s$. Hence, the major difference between the proposed method and RVP-OSS-MPC is listed as follows. Assuming that the OSS at the *k*th control period is $v_{\mathrm{sw}5}$, $\{\boldsymbol{V}_5, \boldsymbol{V}_6, \boldsymbol{V}_0\}$. For RVP-OSS-MPC, after calculating the duty cycles and cost function for $v_{\mathrm{sw}1}$, the duty cycles and cost functions for the other five switching sequences $v_{\mathrm{sw}2}, v_{\mathrm{sw}3}, \ldots, v_{\mathrm{sw}6}$ should also be calculated to find the OSS. However, the duty cycles are calculated for only one switching sequence in the proposed method. After calculating the duty cycles for $v_{\mathrm{sw}1}$, if $(-\varphi d_1 - \varphi d_2) > 0$ and $(\varphi d_1 + (\varphi - 1) d_2) > 0$, the OSS is determined as $v_{\mathrm{sw}5}$, $\{\boldsymbol{V}_5, \boldsymbol{V}_6, \boldsymbol{V}_0\}$, and its duty cycles are reconstructed using (17). Therefore, cost function calculations of six feasible switching sequences using (8)-(9) and duty cycles calculations of the other five switching sequences using (11) are not required in the proposed method. Thus, the computational burden is greatly reduced. Moreover, when the Vienna rectifier operates under balanced dc links, φ is 1, and (17) is simplified to $d_5 = -d_1 - d_2$ and $d_6 = d_1$, which is the same as the one described in [31]. In fact, the space vector diagram of the Vienna rectifier under balanced dc links can be converted to that of a two-level converter by shifting the origin point [7]. However, when the Vienna rectifier operates under unbalanced dc links, the unbalanced factor φ is proposed in this article, and d_5 and d_6 can then be reconstructed similar as in [31].

Based on the above-mentioned analysis, different switching sequences can thus be reconstructed by $\boldsymbol{V}_1$, $\boldsymbol{V}_2$, $\boldsymbol{V}_0$, d_1, d_2, and $(1 - d_1 - d_2)$ as follows:

$$\begin{aligned} & V_1 d_1 + V_2 d_2 + V_0 (1 - d_1 - d_2) \\ & = V_2 (\varphi d_1 + d_2) + V_3 (-\varphi d_1) + V_0 (1 - d_2) \\ & = V_3 d_2 + V_4 (-\varphi d_1 - d_2) + V_0 (1 + \varphi d_1) \\ & = V_4 (-\varphi d_1 + (1 - \varphi) d_2) + V_5 (-d_2) + V_0 (1 + \varphi d_1 + \varphi d_2) \\ & = V_5 (-\varphi d_1 - \varphi d_2) + V_6 (\varphi d_1 + (\varphi - 1) d_2) + V_0 (1 + d_2) \\ & = V_6 (-d_2) + V_1 (d_1 + d_2) + V_0 (1 - d_1). \end{aligned} \tag{18}$$

As seen in (18), different switching sequences can always be equivalently reconstructed by $v_{\mathrm{sw}1}$, $\{\boldsymbol{V}_1, \boldsymbol{V}_2, \boldsymbol{V}_0\}$ with completely different duty cycles. Therefore, by calculating the duty cycles for switching sequence $v_{\mathrm{sw}1}$, $\{\boldsymbol{V}_1, \boldsymbol{V}_2, \boldsymbol{V}_0\}$, the OSS and its duty cycles can always be reconstructed. For better demonstration, the reconstructed OSS and its duty cycles are listed out in Table II.

TABLE II
RECONSTRUCTED SWITCHING SEQUENCE AND DUTY CYCLES

Reconstructed duty cycles	Reconstructed switching sequence
$d_1>0$ & $d_2>0$	v_{sw1}
$\varphi d_1+d_2>0$ &$-\varphi d_1>0$	v_{sw2}
$d_2>0$ & $-\varphi d_1-d_2>0$	v_{sw3}
$-\varphi d_1+(1-\varphi)d_2>0$ &$-d_2>0$	v_{sw4}
$-\varphi d_1-\varphi d_2>0$ & $\varphi d_1+(\varphi-1)d_2>0$	v_{sw5}
$-d_2>0$ & $d_1+d_2>0$	v_{sw6}

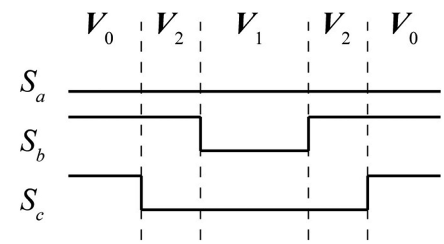

Fig. 4. Switching signal generation in sector I with $v_{\mathrm{sw}1}$ being the OSS.

Following the above-mentioned procedure, the obtained duty cycles are always greater than zero, but their sum may be larger than one. In this case, their sum is saturated to 1. For example, if the OSS is $v_{\mathrm{sw}1}$, $\{\boldsymbol{V}_1, \boldsymbol{V}_2, \boldsymbol{V}_0\}$, and duty cycles of $\boldsymbol{V}_1$ and $\boldsymbol{V}_2$ are d_1 and d_2. If $(d_1 + d_2) > 1$, the optimal duty cycles are saturated to

$$d_1 = d_1 / (d_1 + d_2), d_2 = 1 - d_1. \tag{19}$$

In this case, the duty cycle for $\boldsymbol{V}_0$ is 0, and the Vienna rectifier operates in the overmodulation region, which usually happens when large current reference change occurs. It is noted that, in the overmodulation region, various harmonics are introduced in the ac current, and the system design should avoid the Vienna rectifier operating in the overmodulation region.

3) Switching Sequence Arrangement: Assuming the OSS is $v_{\mathrm{sw}1}$, $\{\boldsymbol{V}_1, \boldsymbol{V}_2, \boldsymbol{V}_0\}$, the double-side switching pattern is adopted according to SVPWM principle, which is depicted in Fig. 4.

4) One-Step Delay Compensation: In digital implementation of the OSS-MPC scheme, there is one-step delay between the commanding voltage vector and the applied vector [36]. To solve this problem, the two-step prediction is adopted. First, assume that the OSS at the *k*th instant is v_{swop}, $\{\boldsymbol{V}_{\mathrm{op}1}, \boldsymbol{V}_{\mathrm{op}2}, \boldsymbol{V}_{\mathrm{op}3}\}$ and their duty cycles are $d_{\mathrm{op}1}$, $d_{\mathrm{op}2}$, and $d_{\mathrm{op}3}$, respectively. The α–β axis voltage components synthesized by v_{swop} are

$$v_{\alpha \mathrm{op}} = \sum_{j=1}^{3} v_{\alpha \mathrm{op}j} d_{\mathrm{op}j}, v_{\beta \mathrm{op}} = \sum_{j=1}^{3} v_{\beta \mathrm{op}j} d_{\mathrm{op}j}. \tag{20}$$

The predicted α–β axis currents at the $(k+1)$th instant are

$$\begin{aligned} i_\alpha(k+1) &= i_\alpha(k) + \frac{T_s}{L}(e_\alpha(k) - R_s i_\alpha(k) - v_{\alpha \mathrm{op}}) \\ i_\beta(k+1) &= i_\beta(k) + \frac{T_s}{L}(e_\beta(k) - R_s i_\beta(k) - v_{\beta \mathrm{op}}). \end{aligned} \tag{21}$$

The predicted current at the $(k+1)$th instant will serve as the initial state of the system to compensate for the one-step delay, and more details can be found in [36].

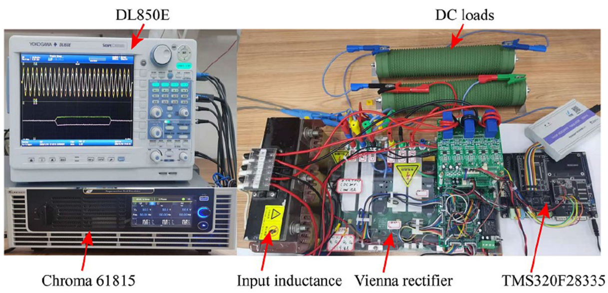

Fig. 5. Photograph of the experimental platform.

TABLE III
SYSTEM PARAMETERS

Parameters	Values
Input line voltage e_a, e_b, e_c (RMS)	110 V
Input angular frequency	314 rad/s
Filter Inductance L	6 mH
Equivalent resistance R_s	0.2 Ω
DC-link capacitance C_1, C_2	C_1=C_2=600 μF
Load resistance R_1, R_2	R_1=R_2=50 Ω
Control period T_s	100 μs

Depending on the polarity of three-phase ac current, there are six sectors in the Vienna rectifier. In each sector, there are two redundant vectors. Hence, there are 12 situations in total for the six sectors and different preselected redundant vectors. The situation in which the Vienna rectifier operates in sector I and $\boldsymbol{V}_0$ is preselected is analyzed above. The other eleven situations can be analyzed similarly, and 11 look-up tables are obtained, which are included in the supplementary material. Finally, these 12 look-up tables are merged into 4, which ensures that the increased memory usage of the proposed method is limited.

IV. Experimental Results

To verify the effectiveness of the proposed computationally efficient OSS-MPC method, experimental studies are conducted, as they can better demonstrate the control performance in the presence of model uncertainty and measurement noise. As shown in Fig. 5, an experimental prototype is built in the laboratory, and the system parameters are enumerated in Table III. The power stage of the Vienna rectifier is constructed with discrete power semiconductors C2M0080120, and is controlled by digital signal processor TMS320F28335. Programmable ac source CHROMA 61815 is adopted as the three-phase power supply, and all the experimental data are recorded by Scopecorder DL850E. The experimental results of the proposed method and those of the RVP-OSS-MPC [21] are presented to demonstrate the superiority of the proposed method.

A. Steady-State Performance Evaluation

First, the steady-state performance of the proposed method and RVP-OSS-MPC under balanced/unbalanced dc links is investigated. Fig. 6 presents the steady-state responses under balanced dc links. It should be noted that the neutral-point voltage is calculated by using the math function of DL850E. In the balanced dc links case, the dc-link voltage reference is 320 V

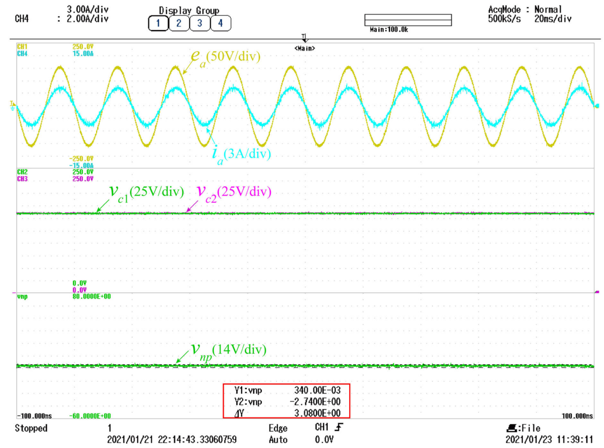

(a)

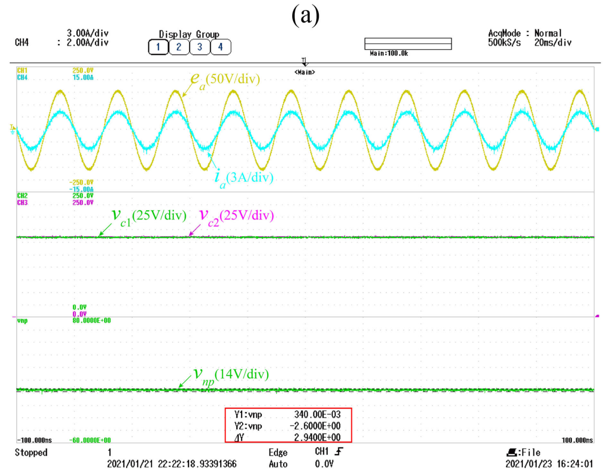

(b)

Fig. 6. Steady-state performance under balanced dc links for (a) proposed method and (b) RVP-OSS-MPC. From top to bottom, waveforms are phase "a" voltage and current, two capacitor voltages, and neutral-point voltage.

and the voltage references for C_1 and C_2 are both 160 V. It is indicated that both methods can achieve good tracking of current references, and the voltages of capacitors C_1 and C_2 are both well-regulated at 160 V. The fluctuations in the neutral-point voltage in the proposed method and RVP-OSS-MPC are approximately 3.08 and 2.94 V, respectively, which shows that the proposed method has similar steady-state performance as RVP-OSS-MPC under balanced dc links. For a better demonstration, the phase "a" current harmonic spectrum of the proposed method and RVP-OSS-MPC under balanced dc links are presented in Fig. 7. It is worthwhile to mention that the current is obtained from DL850E with a sampling frequency of 500 kHz and then analyzed in MATLAB. As shown in Fig. 7, the current THD is 2.83% for the proposed method and 2.87% for RVP-OSS-MPC. Furthermore, the two methods have similar harmonic spectral. Thus, it is concluded that the proposed method is equivalent to RVP-OSS-MPC under balanced dc links.

Fig. 8 shows the steady-state responses of the proposed method and RVP-OSS-MPC under unbalanced dc links. In this case, the neutral-point voltage reference is set to 50 V. Because the dc-link voltage reference is 320 V, the voltage references for C_1 and C_2 are 185 and 135 V, respectively. As shown

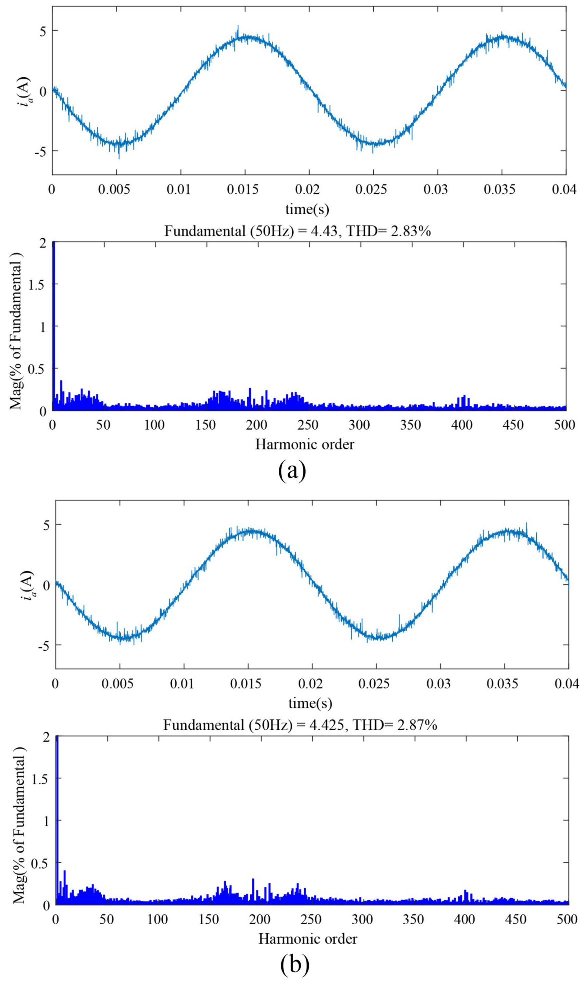

Fig. 7. Phase "a" current and its harmonic spectrum under balanced dc links for (a) proposed method (b) RVP-OSS-MPC.

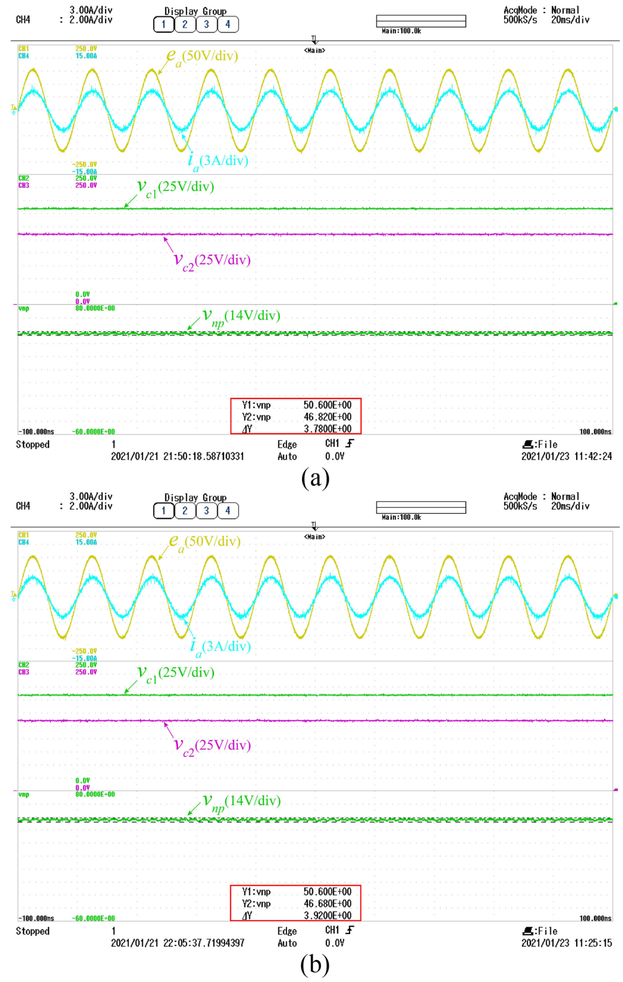

Fig. 8. Steady-state performance under unbalanced dc links for (a) proposed method and (b) RVP-OSS-MPC. From top to bottom, waveforms are phase "a" voltage and current, two capacitor voltages, and neutral-point voltage.

in Fig. 8, v_{c1} and v_{c2} in both methods are well-regulated at 185 V and 135 V, respectively. The fluctuations of neutral-point voltage in the proposed method and RVP-OSS-MPC are about 3.78 V and 3.92 V, respectively. It is noted that the neutral-point voltage fluctuation under unbalanced dc links is slightly larger than that under balanced dc links. The main reason for this phenomenon is that the Vienna rectifier has limited capability of unbalanced loads [8], [37]. However, this problem can be solved by adding balancers into the Vienna rectifier to allocate power flow between the output loads [13], which is out of the scope of this article and is thus not expanded further. The phase "a" current harmonic spectrum of the two methods under unbalanced dc links is shown in Fig. 9. The current THD is 2.85% and 2.88% for the proposed method and RVP-OSS-MPC, respectively. The proposed method and RVP-OSS-MPC have similar steady-state performance under unbalanced dc links. Hence, the above-mentioned results confirm the equivalence between the proposed method and RVP-OSS-MPC under balanced and unbalanced dc links.

Although the proposed method achieves the same steady-state performance as that achieved by RVP-OSS-MPC, the computational burden of the proposed method is significantly reduced, as the enumeration process in RVP-OSS-MPC is eliminated. It is noted that balanced dc links ($\varphi = 1$) can be considered a special case of unbalanced dc links, so only the calculation time of the proposed method under unbalanced dc links is given in this article. The computational burden of the proposed method and RVP-OSS-MPC is tested on the same hardware, DSP TMS320F28335 running at 150 MHz, and their execution times are 4.7 and 24.6 μs for the proposed method and RVP-OSS-MPC, respectively. Therefore, compared with RVP-OSS-MPC, the execution time of the proposed method is significantly reduced by approximately 80.9% [(24.6−4.7)/24.6 = 80.9%], and the steady-state performance is not sacrificed.

B. Dynamic Performance Evaluation

In addition to the steady-state performance evaluation, the dynamic performance evaluation of the proposed method and RVP-OSS-MPC is also conducted.

To evaluate the performance of the neutral-point voltage controller in the proposed method and RVP-OSS-MPC when a sudden dc load change occurs, a 100-Ω load parallel to R_2 is suddenly connected to C_2. In this case, the dc-link voltage

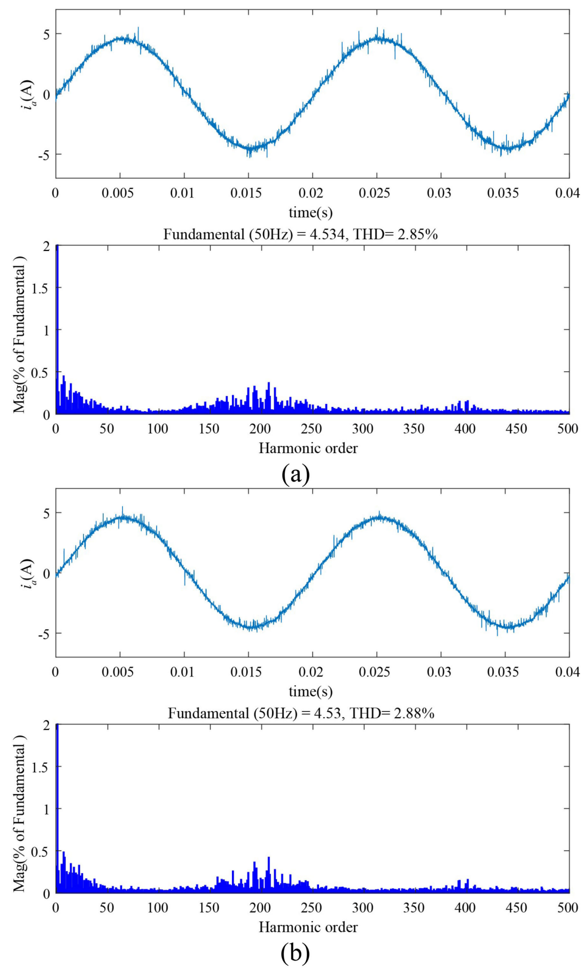

Fig. 9. Phase "a" current and its harmonic spectrum under unbalanced dc links for (a) proposed method and (b) RVP-OSS-MPC.

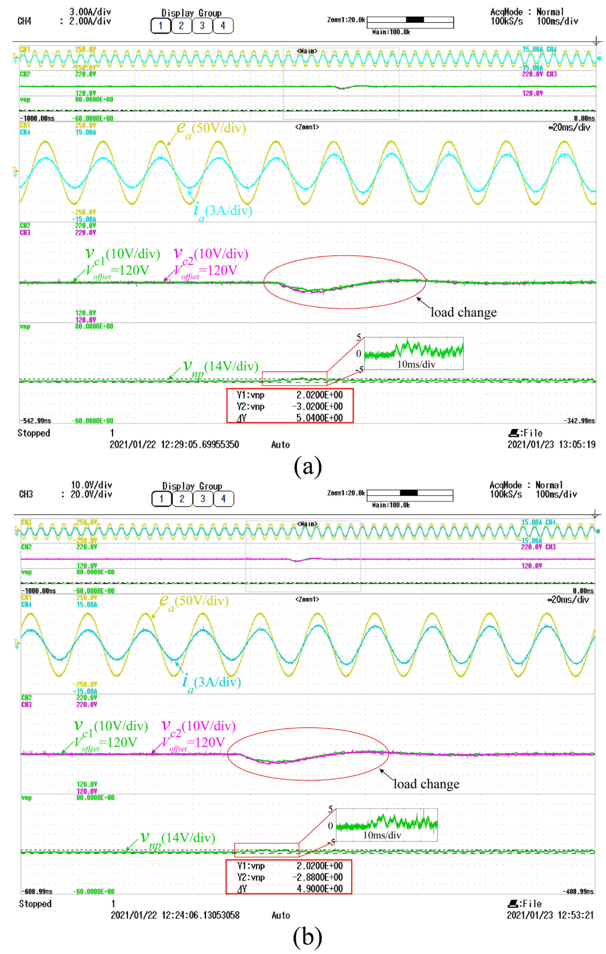

Fig. 10. Dynamic performance to dc load change under balanced dc links for (a) proposed method and (b) RVP-OSS-MPC. From top to bottom, waveforms are phase "a" voltage and current, two capacitor voltages, and neutral-point voltage.

reference is kept at 320 V. Fig. 10 presents the dynamic responses of the dc load change for both methods under balanced dc links. As shown in Fig. 10, when the 100-Ω load is connected, a small drop is observed on both capacitor voltages. Then, the neutral-point voltage increases to approximately 4 V in both methods. Finally, the neutral-point voltage in both methods recovers to zero in less than 0.02 s, exhibiting strong robustness against sudden load disturbances. Moreover, the fluctuations in the neutral-point voltage using the proposed method and RVP-OSS-MPC are approximately 5.04 V and 4.90 V, respectively. Fig. 11 shows the dynamic responses of the dc load change for the two methods under unbalanced dc links. As seen in Fig. 11, the neutral-point voltages in both methods are well-regulated at 50 V, and the fluctuations of the neutral-point voltage for the proposed method and RVP-OSS-MPC are approximately 4.76 and 4.62 V, respectively. Hence, the neutral-point voltage controllers of the proposed method and RVP-OSS-MPC are effective when a sudden dc load change occurs.

The dynamic responses of dc-link voltage reference change for the proposed method and RVP-OSS-MPC are also tested. In this case, the dc-link voltage reference changes from 320 to 350 V. It is worthwhile to mention that the outer PI controller parameters used in both methods are the same. In Fig. 12, the Vienna rectifier operates under balanced dc links. Thus, the voltage references for C_1 and C_2 are initially both 160 V and are then changed to 175 V. As observed in Fig. 12, the proposed method and RVP-OSS-MPC track the dc-link voltage reference change within 66.1 and 64.8 ms, respectively. Besides, the neutral-point voltage is effectively regulated in both methods. Fig. 13 shows the dynamic responses of dc-link voltage reference change under unbalanced dc links. Because the neutral-point voltage reference is 50 V, the voltage references for C_1 and C_2 are 185 and 135 V initially, and are then changed to 200 and 150 V, respectively. As seen in Fig. 13, both capacitor voltages are well-regulated. The proposed method and RVP-OSS-MPC track the dc-link voltage reference change within 57.2 and 59.8 ms, respectively. The above results also verify the equivalence between the two methods.

In Fig. 14, the dc links are set to be balanced at first, then unbalanced, and finally balanced again. The balanced and unbalanced dc links are obtained by setting neutral-point voltage reference to 0 and 50 V, respectively. As shown in Fig. 14, the capacitor voltages are well-regulated in both methods, indicating the

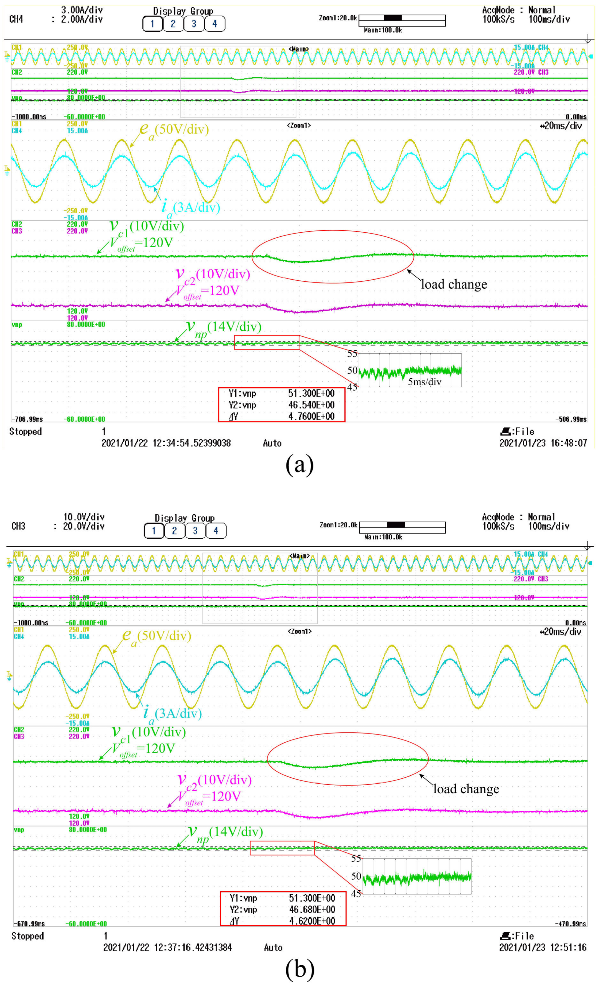

Fig. 11. Dynamic performance to dc load change under unbalanced dc links for (a) proposed method and (b) RVP-OSS-MPC. From top to bottom, waveforms are phase "a" voltage and current, two capacitor voltages, and neutral-point voltage.

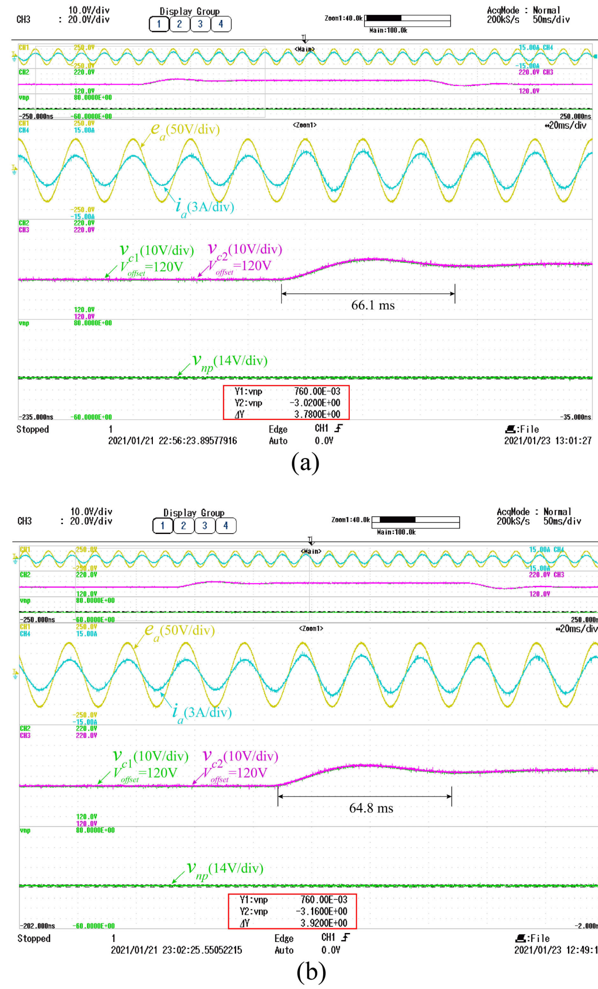

Fig. 12. Dynamic performance to dc-link voltage reference change under balanced dc links for (a) proposed method and (b) RVP-OSS-MPC. From top to bottom, waveforms are phase "a" voltage and current, two capacitor voltages, and neutral-point voltage.

effectiveness of the neutral-point voltage control method. Furthermore, the neutral-point voltage tracks the reference change within 25.00 ms for the proposed method and within 24.85 ms for RVP-OSS-MPC, which further proves the equivalence between the proposed method and RVP-OSS-MPC.

C. Comparison With Several Computational Burden Reduction Methods

The comparison is carried out from two aspects: the computational burden and the steady-state performance.

To evaluate the computational burden of the proposed method, the execution time of RVP-OSS-MPC [21], the proposed method, CFM-MPC [20], and low complexity MPC (LC-MPC) [27] are measured using a CPU timer of DSP TMS320F28335, and the results are presented in Table IV. For a fair comparison, only the time required by the predictive control algorithm is considered. It costs 24.6, 4.7, 10.3, and 3.43 μs to implement RVP-OSS-MPC, the proposed method, CFM-MPC, and LC-MPC, respectively. As the RVP-OSS-MPC needs seven current slope calculations [see (7)], six duty cycle calculations [see (11)], six current predictions [see (8)], and six cost function calculations and comparisons [see (9)], it requires the longest execution time and needs 24.6 μs to realize the predictive control algorithm. To reduce the computational burden, four look-up tables are established in the proposed method. Three current slope calculations (two adjacent nonredundant vectors and one preselected redundant vector), one duty cycle calculation, and one duty cycle reconstruction [see (18)] are required. Thus, the execution time of the proposed method is reduced to 4.7 μs. For the CFM-MPC, one reference voltage vector calculation, one sector determination, four current slope calculations, four cost function calculations, and one duty cycle calculation are required. Although a simplified duty cycle derivation method is adopted, the execution time of CFM-MPC is 10.3 μs, which is

TABLE IV
EXECUTION TIME FOR DIFFERENT MPC ALGORITHMS

Method	RVP-OSS-MPC [21]	Proposed method	CFM-MPC [20]	LC-MPC [27]
Execution time	24.6 μs	4.7 μs	10.3 μs	3.43 μs

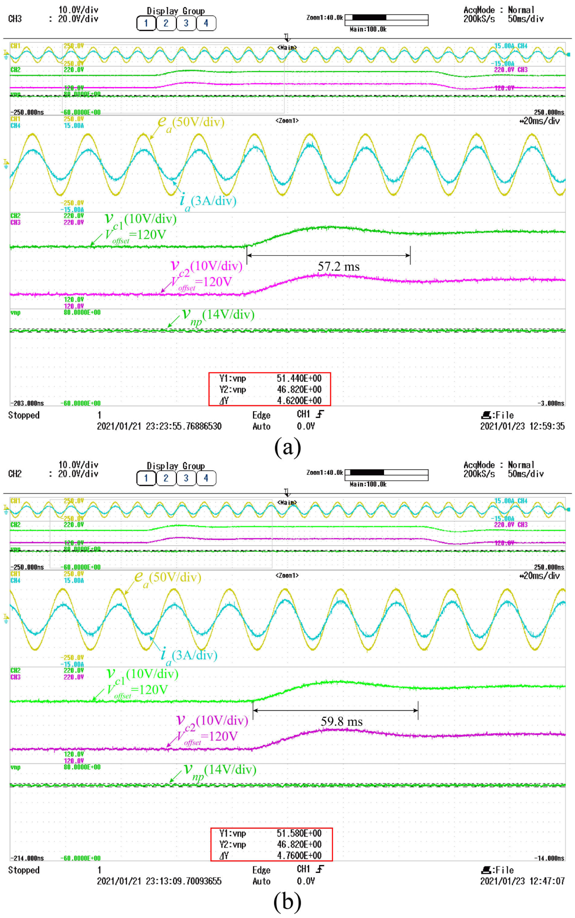

Fig. 13. Dynamic performance to dc-link voltage reference change under unbalanced dc links for (a) proposed method and (b) RVP-OSS-MPC. From top to bottom, waveforms are phase "a" voltage and current, two capacitor voltages, and neutral-point voltage.

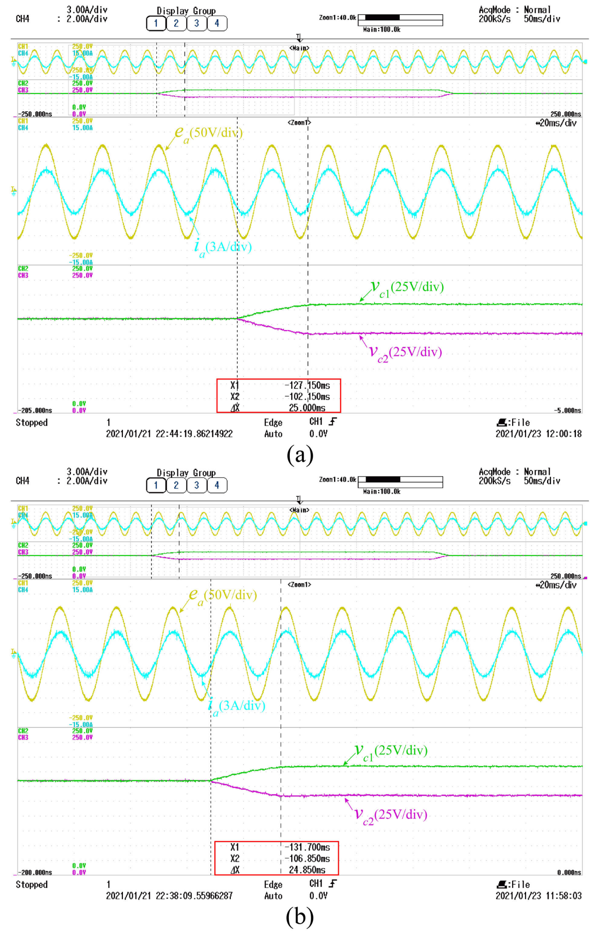

Fig. 14. Dynamic performance to neutral-point voltage reference change for (a) proposed method and (b) RVP-OSS-MPC. From top to bottom, waveforms are phase "a" voltage and current, and two capacitor voltages.

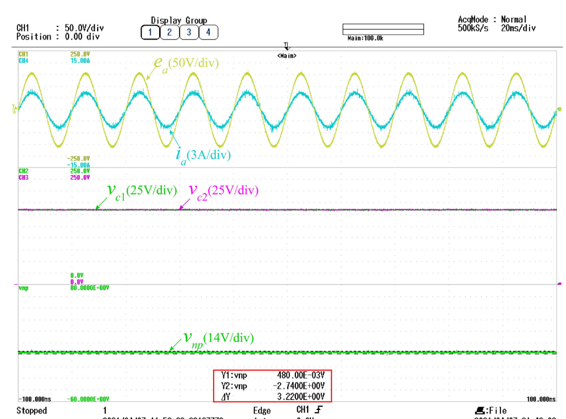

Fig. 15. Steady-state performance under balanced dc links for the LC-MPC. From top to bottom, waveforms are phase "a" voltage and current, two capacitor voltages, and neutral-point voltage.

larger than that of the proposed method. For the LC-MPC, one reference voltage vector calculation, one sector determination, and one duty cycle calculation are required. The execution time of LC-MPC is 3.43 μs, which is smaller than that of the proposed method. However, considering the 100-μs sampling period, the proposed method and LC-MPC show similar performance in terms of the computational burden.

To verify the validity of the proposed method, the steady-state performance of LC-MPC is also investigated. Fig. 15 presents the steady-state responses of the LC-MPC under balanced dc links. In this case, the dc-link voltage reference is 320 V and the voltage references for C_1 and C_2 are both 160 V. The phase "a" current harmonic spectrum of the LC-MPC is shown in Fig. 16. As seen in Figs. 7 and 16, the current THD is 2.83% and 2.89% for the proposed method and LC-MPC, respectively. Thus, the proposed method and LC-MPC have similar steady-state performance under balanced dc links.

Fig. 17 presents the steady-state responses of the LC-MPC under unbalanced dc links, where the neutral-point voltage reference is set to 50 V. As the dc-link voltage reference is 320 V, the voltage references for C_1 and C_2 are 185 V and 135 V, respectively. The phase "a" current harmonic spectrum of the LC-MPC is shown in Fig. 18. As seen in Figs. 9 and 18, the current THD is 2.85% and 5.31% for the proposed method and LC-MPC, respectively. Moreover, the LC-MPC contains more low-order harmonics than the proposed method. This is because a nonoptimal switching sequence is frequently selected in the LC-MPC due to the asymmetric space-vector diagram. To solve

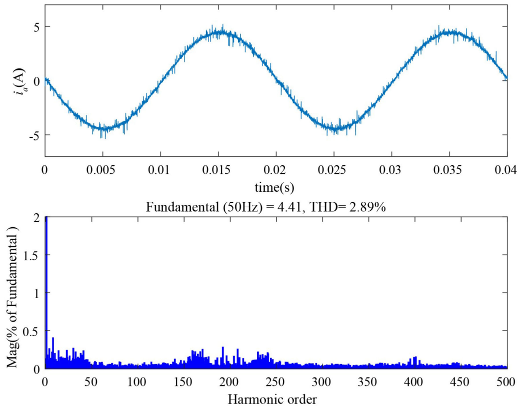

Fig. 16. Phase "a" current and its harmonic spectrum under balanced dc links for the LC-MPC.

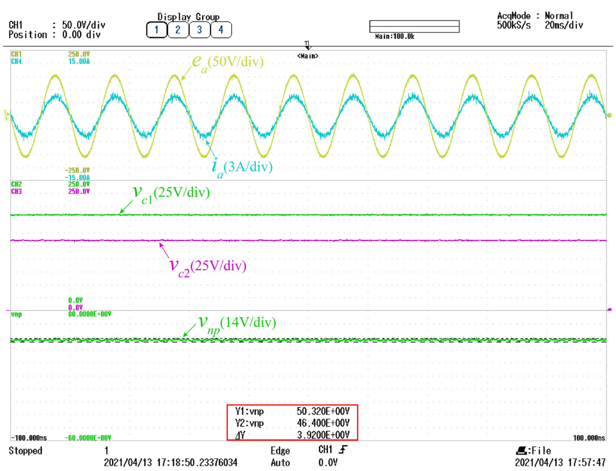

Fig. 17. Steady-state performance under unbalanced dc links for the LC-MPC. From top to bottom, waveforms are phase "a" voltage and current, two capacitor voltages, and neutral-point voltage.

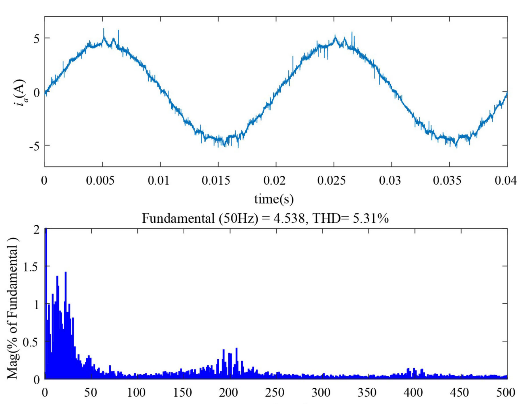

Fig. 18. Phase "a" current and its harmonic spectrum under unbalanced dc links for the LC-MPC.

this problem, an unbalanced factor is proposed in this article. The OSS and its duty cycles are correctly reconstructed. Thus, compared with the LC-MPC, the proposed method achieves better current quality under unbalanced dc links.

To further validate the steady-state performance improvement of the proposed method under unbalanced dc links, quantitative

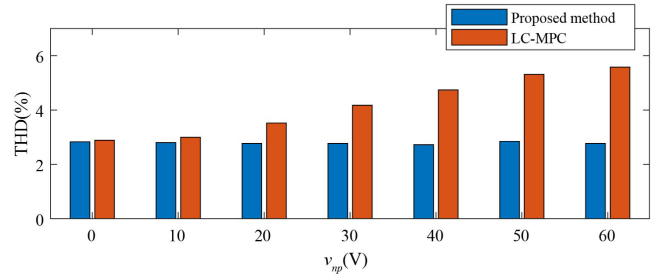

Fig. 19. Quantitative comparison of phase "a" current THD at various neutral-point voltage for the proposed method and LC-MPC.

comparison of phase "a" current THD for the proposed method and LC-MPC is presented in Fig. 19, where the neutral-point voltage varies from 0 to 60 V. As the neutral-point voltage increases, the current quality of the proposed method almost keeps constant, whereas the current quality of the LC-MPC becomes worse. This further verifies the effectiveness of the proposed method in current quality improvement under unbalanced dc links.

V. Conclusion

This article proposes a computationally efficient OSS-MPC scheme for a three-phase Vienna rectifier under balanced and unbalanced dc links. The neutral-point voltage is regulated by redundant vector preselection, and the weighting factor is eliminated. As for ac current control, 12 situations are obtained with different sectors and preselected redundant vectors. In each situation, an unbalanced factor is proposed to describe the equivalence relation among the six feasible switching sequences under balanced/unbalanced dc links. Hence, the proposed method only needs to calculate the duty cycles for one switching sequence, and the OSS and its duty cycles are reconstructed based on the predefined table. Compared with RVP-OSS-MPC, the proposed method eliminates the enumeration process of duty cycle calculation and cost function evaluation, so the computational burden is significantly reduced. Compared with other computational burden reduction methods, the proposed method can always correctly reconstruct the OSS and its duty cycles, so better current quality is obtained under unbalanced dc links. The experimental results verify the effectiveness and advantages of the proposed method.

References

[1] J. W. Kolar and F. C. Zach, "A novel three-phase utility interface minimizing line current harmonics of high-power telecommunications rectifier modules," *IEEE Trans. Ind. Electron.*, vol. 44, no. 4, pp. 456–466, Aug. 1997.

[2] B. Kedjar, H. Y. Kanaan, and K. Al-Haddad, "Vienna rectifier with power quality added function," *IEEE Trans. Ind. Electron.*, vol. 61, no. 8, pp. 3847–3856, Aug. 2014.

[3] J. Lee, K. Lee, and F. Blaabjerg, "Predictive control with discrete space-vector modulation of Vienna rectifier for driving PMSG of wind turbine systems," *IEEE Trans. Power Electron.*, vol. 34, no. 12, pp. 12368–12383, Dec. 2019.

[4] J. Lee and K. Lee, "Carrier-based discontinuous PWM method for Vienna rectifiers," *IEEE Trans. Power Electron.*, vol. 30, no. 6, pp. 2896–2900, Jun. 2015.

[5] J. Lee and K. Lee, "A novel carrier-based PWM method for Vienna rectifier with a variable power factor," *IEEE Trans. Power Electron.*, vol. 63, no. 1, pp. 3–12, Jan. 2016.

[6] W. Zhu, C. Chen, S. Duan, T. Wang, and P. Liu, "A carrier-based discontinuous PWM method with varying clamped area for Vienna rectifier," *IEEE Trans. Ind. Electron.*, vol. 66, no. 9, pp. 7177–7188, Sep. 2019.

[7] R. Burgos, R. Lai, Y. Pei, F. Wang, D. Boroyevich, and J. Pou, "Space vector modulator for Vienna-type rectifiers based on the equivalence between two- and three-level converters: A carrier-based implementation," *IEEE Trans Power Electron,* vol. 23, no. 4, pp. 1888–1898, Jul. 2008.

[8] L. Hang, M. Zhang, B. Li, L. Huang, and S. Liu, "Space vector modulation strategy for VIENNA rectifier and load unbalanced ability," *IET Power Electron.*, vol. 6, no. 7, pp. 1399–1405, Aug. 2013.

[9] Z. Ye, Y. Xu, X. Wu, G. Tan, X. Deng, and Z. Wang, "A simplified PWM strategy for a neutral-point-clamped (NPC) three-level converter with unbalanced DC links," *IEEE Trans. Power Electron.*, vol. 31, no. 4, pp. 3227–3238, Apr. 2016.

[10] H. Wu, J. Wang, T. Liu, and Y. Xing, "Modified SVPWM controlled three port three-phase AC-DC converters with reduced power conversion stages for wide voltage range applications," *IEEE Trans. Ind. Electron.*, vol. 33, no. 8, pp. 6672–6686, Aug. 2018.

[11] X. Wu, G. Tan, G. Yao, C. Sun, and G. Liu, "A hybrid PWM strategy for three-level inverter with unbalanced dc links," *IEEE J. Emerg. Sel. Top. Power Electron.*, vol. 6, no. 1, pp. 1–15, Mar. 2018.

[12] W. Ding, C. Zhang, F. Gao, B. Duan, and H. Qiu, "A zero-sequence component injection modulation method with compensation for current harmonic mitigation of Vienna rectifier," *IEEE Trans. Power Electron.*, vol. 34, no. 1, pp. 801–814, Jan. 2019.

[13] W. Ding, H. Qiu, B. Duan, X. Xing, N. Cui, and C. Zhang, "A novel segmented component injection scheme to minimize the oscillation of dc-link voltage under balanced and unbalanced conditions for Vienna rectifier," *IEEE Trans. Power Electron.*, vol. 34, no. 10, pp. 9536–9551, Oct. 2019.

[14] D. Zhou, L. Ding, and Y. R. Li, "Two-stage model predictive control of neutral-point-clamped inverter-fed permanent-magnet synchronous motor drives under balanced and unbalanced DC links," *IEEE Trans. Ind. Electron.*, vol. 68, no. 5, pp. 3750–3759, May 2021.

[15] X. Li, Y. Sun, H. Wang, M. Su, and S. Huang, "A hybrid control scheme for three-phase Vienna rectifiers," *IEEE Trans. Power Electron.*, vol. 33, no. 1, pp. 629–640, Jan. 2018.

[16] S. M. H. Khorasgani, A. Izadinia, and H. R. Karshenas, "Finite control set model predictive control for dc voltage balancing in Vienna rectifier," in *Proc. 24th Iranian Conf. Elect. Eng.*, 2016, pp. 687–692.

[17] A. Rajaei, M. Mustafa, and A. Y. Varjani, "Vienna-rectifier-based direct torque control of PMSG for wind energy application," *IEEE Trans. Ind. Electron.*, vol. 60, no. 7, pp. 2919–2929, Jul. 2013.

[18] J. S. Lee and K. B. Lee, "Predictive control of Vienna rectifiers for PMSG systems." *IEEE Trans. Ind. Electron.*, vol. 64, no. 4, pp. 2580–2591, Apr. 2017.

[19] S. Y. Yip, H. S. Che, C. P. Tan, and W. T. Chong, "A lookup table model predictive direct torque control of permanent-magnet synchronous generator based on Vienna rectifier," *IEEE J. Emerg. Sel. Top. Power Electron.*, vol. 8, no. 2, pp. 1208–1222, Jun. 2020.

[20] C. Dang, X. Tong, W. Song, Y. Han, and P. Wheeler, "Cost function-based modulation scheme of model predictive control for VIENNA rectifier," *IET Power Electron.*, vol. 12, no. 14, pp. 3646–3655, Oct. 2019.

[21] S. Xie, Y. Sun, M. Su, J. Lin, and Q. Guang, "Optimal switching sequence model predictive control for three-phase Vienna rectifiers," *IET Electr. Power Appl.*, vol. 12, no. 7, pp. 1006–1013, Aug. 2018.

[22] C. Rojas, J. Rodriguez, F. Villarroel, J. Espinoza, C. Silva, and M. Trincado, "Predictive torque and flux control without weighting factors," *IEEE Trans. Ind. Electron.*, vol. 60, no. 2, pp. 681–690, Feb. 2013.

[23] X. Wang and D. Sun, "Three-vector-based low-complexity model predictive direct power control strategy for doubly fed induction generators," *IEEE Trans. Power Electron.*, vol. 32, no. 1, pp. 773–782, Jan. 2017.

[24] A. Bahrami, M. Norambuena, M. Narimani, and J. Rodriguez, "Model predictive current control of a seven-level inverter with reduced computational burden," *IEEE Trans. Power Electron.*, vol. 35, no. 6, pp. 5729–5740, Jun. 2020.

[25] S. Kang, J. Soh, and R. Kim, "Symmetrical three-vector-based model predictive control with deadbeat solution for IPMSM in rotating reference frame," *IEEE Trans. Ind. Electron.*, vol. 67, no. 1, pp. 159–168, Jan. 2020.

[26] B. Wang, Z. Dong, Y. Yu, G. Wang, and D. Xu, "Static-errorless deadbeat predictive current control using second-order sliding-mode disturbance observer for induction machine drives," *IEEE Trans. Power Electron.*, vol. 33, no. 3, pp. 2395–2403, Mar. 2018.

[27] Q. Wang *et al.*, "A low-complexity optimal switching time-modulated model-predictive control for PMSM with three-level NPC converter," *IEEE Trans. Transp. Electrific.*, vol. 6, no. 3, pp. 1188–1198, Sep. 2020.

[28] Y. Zhang, D. Xu, and L. Huang, "Generalized multiple-vector-based model predictive control for PMSM drives," *IEEE Trans. Ind. Electron.*, vol. 65, no. 12, pp. 9356–9366, Dec. 2018.

[29] A. Mora, R. Cárdenas-Dobson, R. P. Aguilera, A. Angulo, F. Donoso, and J. Rodriguez, "Computationally efficient cascaded optimal switching sequence MPC for grid-connected three-level NPC converters," *IEEE Trans. Power Electron.*, vol. 34, no. 12, pp. 12464–12475, Dec. 2019.

[30] A. Mora, R. Cardenas, R. Aguilera, A. Angulo, P. Lezana, and D. D. Lu, "Predictive optimal switching sequence direct power control for grid-tied 3L-NPC converters," *IEEE Trans. Ind. Electron.*, to be published.

[31] Z. Song, W. Chen, and C. Xia, "Predictive direct power control for three-phase grid-connected converters without sector information and voltage vector selection," *IEEE Trans. Power Electron.*, vol. 29, no. 10, pp. 5518–5531, Oct. 2014.

[32] X. Shi, J. Zhu, L. Li, D. D.-C. Lu, J. Zhang, and H. Yang, ''Predictive duty cycle control with reversible vector selection for three-phase AC/DC converters," *IEEE Trans. Power Electron.*, vol. 34, no. 5, pp. 4868–4882, May 2019.

[33] M. Li, X. Wu, S. Huang, and G. Liang, "Model predictive direct power control using optimal section selection for PWM rectifier with reduced calculation burden," *Int. J. Electr. Power Energy Syst.*, vol. 116, Mar. 2020, Art. no. 105552.

[34] B. Wu and M. Narimani, *High-power Converters and AC Drives*, vol. 59. Hoboken, NJ, USA: Wiley, 2017.

[35] Y. Yang *et al.*, "Multiple-voltage-vector model predictive control with reduced complexity for multilevel inverters," *IEEE Trans. Transp. Electrific.*, vol. 6, no. 1, pp. 105–117, Mar. 2020.

[36] P. Cortes, J. Rodriguez, C. Silva, and A. Flores, "Delay compensation in model predictive current control of a three-phase inverter," *IEEE Trans. Ind. Electron.*, vol. 59, no. 2, pp. 1323–1325, Feb. 2012.

[37] L. Zhang *et al.*, "A modified DPWM with neutral point voltage balance capability for three-phase Vienna rectifiers," *IEEE Trans. Power Electron.*, vol. 36, no. 1, pp. 263–273, Jan. 2021.

Bo Xu was born in Jiangxi, China, in 1995. He received the B.S. degree in electrical engineering from Xiamen University, Xiamen, China, in 2016. He is currently working toward the Ph.D. degree in electrical engineering with Wuhan University, Wuhan, China.

His current research interests include model predictive control for power converters.

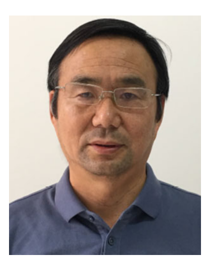

Kaipei Liu was born in Jingmen, Hubei, in 1962. He received the Ph.D. degree in applied computer technology from Wuhan University, Wuhan, China, in 2001.

He is currently a Professor with Wuhan University. His main research fields involve FACTS technology, power quality control and analysis, smart grid as well as the sustainable energy power generation, and connection technologies.

Xiaohong Ran (Member, IEEE) was born in Chongqing. He received the Ph.D. degree in electrical power engineering from Huazhong University of Science and Technology, Wuhan, China, in 2015.

Since 2015, he has been with the School of Electrical Engineering and Automation, Wuhan University, Wuhan, China. He is currently a Visiting Researcher of the field of modeling and control for the ac–dc converters with the Georgia Institute of Technology, Atlanta, GA, USA. His current research interests include the control of power electronics converters applied to renewable energy technology, dc power grid/dc–dc converters, parameter identification, and interval optimization of power systems.